Surface-structural analysis by use of spin-polarized low-energy electron diffraction: An investigation of the Cu(100) surface

D. M. Lind,* F. B. Dunning, and G. K. Walters
Departments of Physics and of Space Physics and Astronomy, and the Rice Quantum Institute, Rice University, Houston, Texas 77251

H. L. Davis
Solid State Division, Oak Ridge National Laboratory, Oak Ridge, Tennessee 37831
(Received 5 January 1987)

A detailed theoretical and experimental study of the Cu(100) surface using spin-polarized low-energy electron diffraction (SPLEED) is reported. An R-factor analysis of the present SPLEED data for the 10, 20, and $1\bar{1}$ beams provides evidence of multilayer relaxation in Cu(100), and suggests that the first and second interlayer spacings deviate by -1.2% and $+0.9\%$, respectively, from the bulk value. The present structural conclusions are in accord with those deduced in earlier LEED I-V studies, and suggest that combined measurements of spin-asymmetry and intensity profiles should provide an improved basis for structure determinations on surfaces of greater complexity.

I. INTRODUCTION

Surface structures are frequently deduced by comparing experimentally determined low-energy electron diffraction (LEED) intensity-versus-energy (I-V) profiles with those calculated using a range of assumed surface structural models. Such comparisons have been aided in recent years by the development of more efficient numerical techniques and computer codes and by the introduction of reliability factors (R factors).[1-5] These advances make possible very detailed interpretation of experimental I-V profiles and enable the evaluation of increasingly sophisticated surface models that incorporate effects such as multilayer relaxation, surface rippling, and reconstruction.

With the advent of the GaAs polarized electron source,[6] it is now possible to measure not only the intensities of diffracted LEED beams but also how these intensities depend on the spin polarization of the incident electrons. In the case of nonmagnetic surfaces these spin dependences result from the spin-orbit effect and provide an additional test of surface structural models in that these must now predict correctly both beam intensities and their polarization dependences.[7]

In the present paper the results of a detailed experimental and theoretical spin-polarized LEED (SPLEED) study of the Cu(100) surface are described.[8] Cu(100) was selected because it has been studied extensively using a variety of surface analytic techniques and a very detailed structural model of the surface has been developed by analysis of LEED I-V profiles.[4,5] This model reflects a surface with multilayer relaxation, but no reconstruction, and gives the atomic spacings to within ~ 0.01 Å. The present work provides an additional test of this structural model, and serves as a quantitative benchmark in exploring the potential of SPLEED for improved structural determinations of more complicated surfaces. Polarization and intensity studies naturally complement one another in that they depend in different ways on the scattering potential, and polarization profiles, tend to emphasize regions of (E,θ,ϕ) space of lower intensity.

Experimental SPLEED data are presented for the 10, $\bar{1}0$, 20, and $1\bar{1}$ beams at normal incidence.[9] These data are compared by means of an R-factor analysis with the results of fully relativistic dynamical calculations. The calculations show that polarization effects are quite sensitive to the assumed surface structure and demonstrate that SPLEED measurements are of value in surface structure determinations. The surface structure derived through analysis of the present SPLEED data is in good agreement with that determined in earlier LEED I-V studies.

II. EXPERIMENTAL TECHNIQUE AND RESULTS

The apparatus used in the present experiment is shown schematically in Fig. 1 and is similar to that employed in earlier SPLEED investigations in this laboratory.[8,10,11] In this apparatus a beam of spin-polarized electrons from a GaAs source is directed at the target surface and the spin dependence of the intensities of the diffracted beams is measured. This spin dependence is specified by means of

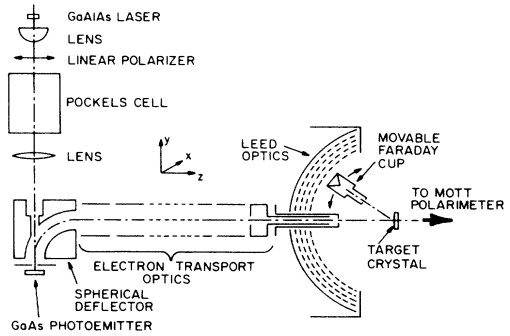

FIG. 1. Schematic diagram of the apparatus.

a spin-asymmetry parameter $A(E,\theta)$:

$$A(E,\theta)=\frac{1}{|P_0|}\frac{I(P_0)-I(-P_0)}{I(P_0)+I(-P_0)}, \quad (1)$$

where P_0 is the spin polarization of the incident electron beam and $I(P_0)$ and $I(-P_0)$ are the scattered intensities with the incident electron spins polarized parallel and antiparallel, respectively, to the y axis defined in Fig. 1. A laboratory-fixed quantization axis is convenient here because, for the $1\bar{1}$ beam data, the incident electron polarization is not perpendicular to the scattering plane.

The polarized electron source is similar to that described by Pierce *et al.*[6] Circularly polarized 807-nm radiation from a $Ga_{1-x}Al_xAs$ diode laser is directed at normal incidence onto a room-temperature GaAs(100) surface that has been treated by cesiumation and oxygenation to obtain negative electron affinity. Photoelectrons ejected from the GaAs surface by the incident radiation are longitudinally polarized. These electrons are accelerated and directed through a 90° electrostatic deflector. The emergent electrons, now transversely polarized, are focused by a series of electron lenses onto the target surface. The incident current at the target is ~ 0.2 to 0.4 μA. The polarization P_0 of the incident beam, measured directly by moving the target crystal so the beam can enter a Mott polarimeter,[11] is $28\pm 2\%$. The polarization can be simply reversed $P_0 \rightarrow -P_0$, without influencing the beam current or trajectory, by changing the sense of circular polarization of the radiation incident on the GaAs photocathode. In practice, the sense of circular polarization is modulated at 500 Hz using a Pockels's cell. This makes possible the simultaneous measurement of the spin-asymmetry parameter and the spin-averaged intensity for each diffracted beam. The beam intensities are measured using a movable Faraday cup. The ac component in the collected current, which is measured using phase-sensitive detection techniques, gives directly the spin dependence of the scattered intensity [i.e., $I(P_0)-I(-P_0)$]. The average dc current into the Faraday cup is measured in parallel by use of an electrometer and provides the spin-averaged intensity (i.e., $[I(P_0)+I(-P_0)]/2$). These two quantities, together with the known incident beam polarization, are used to derive the spin asymmetry parameters $A(E,\theta)$.

The Cu(100) crystal was cut from the same boule as those used in earlier LEED intensity studies by Noonan and Davis.[4,5] The crystal is affixed to the end of a thin molybdenum can that contains an electrically isolated tungsten filament used to heat the can, and thus the crystal, either radiatively or by electron bombardment. The sample surface was prepared by sputtering for ~ 30 min with 750-eV argon ions at a time-averaged current density of $\sim 30\ \mu A\,cm^{-2}$ following by annealing to ~ 500–$550\,^{\circ}C$ for 30 min. Auger analysis showed that no detectable contaminants remained on the surface following this treatment and the observed sharp LEED pattern indicates that the surface is well ordered. Although copper is relatively inert and remains clean under UHV conditions for extended periods of time, the sample was routinely cleaned and annealed before each data acquisition run.

SPLEED measurements are somewhat less susceptible to systematic errors than are LEED intensity measurements. This results because the spin-asymmetry parameter is a current *ratio*, thereby eliminating the possibility of systematic errors associated with absolute measurement of either the incident or diffracted beam currents. Care was taken, however, to test for, and eliminate, other potential sources of systematic error.

In regions of intensity minima, a small, but significant, contribution to the Faraday cup current can result from diffuse scattering. This background, which was observed experimentally to be spin independent and spatially uniform, was measured by positioning the Faraday cup adjacent to the beam of interest so only diffusely scattered electrons could enter. Beam currents and spin dependences recorded with the Faraday cup centered on the diffracted beam was then corrected for this background.

Measurements on the complementary 10 and $\bar{1}0$ beams provide a convenient test of crystal orientation. The scattering geometry in the present experiment is such that the defined spin quantization axis, i.e., the y axis in Fig. 1, is aligned with the 01 direction in the crystal face. Symmetry considerations therefore require that, for normal incidence, the 10 and $\bar{1}0$ beams should have spin-asymmetry parameters that are equal in magnitude but opposite in sign.[12] The measured asymmetry parameter-versus-energy (A-V) profiles for these beams are shown in Fig. 2. Each profile in this figure (and others) is the statistical average of data obtained in a number of independent experimental runs. The vertical extent of each data point in these (and other) A-V profiles represents the standard deviation about the mean of the asymmetry values recorded at each energy on several separate data acquisition runs and therefore reflects not only the statistical uncertainties associated with individual measurements but also the run-to-run reproducibility of the data. The electron energies are corrected for the work function difference between the GaAs photocathode (~ 0 eV) and the Cu(100) surface (~ 4.59 eV) and therefore gives the mean kinetic energy of the incident electrons in vacuum. The A-V pro-

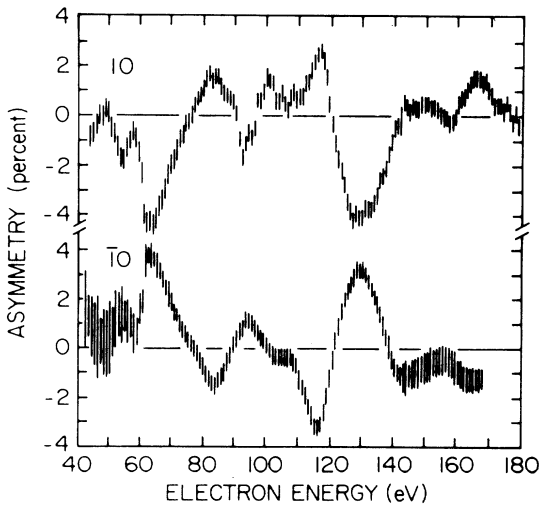

FIG. 2. Comparison of the A-V profiles for the 10 and $\bar{1}0$ beams from Cu(100) at normal incidence.

files in Fig. 2 clearly display the expected asymmetry and confirm that the electron beam is incident normally on the face of the crystal.

A-V profiles for the 10, $1\bar{1}$, and 20 beams at normal incidence are presented in Fig. 3. The best theoretical fits, obtained using the procedures described in the following paragraphs (Sec. III) are also included for comparison. The 10 profile shown is the statistical average of the 10 and (inverted) $\bar{1}0$ data. The magnitudes of the observed asymmetry features are small, typically $\lesssim 6$—$8\,\%$, but are nonetheless very reproducible. Their small size is not unexpected given the low atomic number ($Z=29$) of copper, which results in a relatively weak spin-orbit interaction. The corresponding *I-V* profiles are shown in Fig. 4 together with those reported by other workers.[4,5] The positions and shapes of the present intensity features are in good agreement with those observed in earlier investigations. The differences in relative peak heights re-

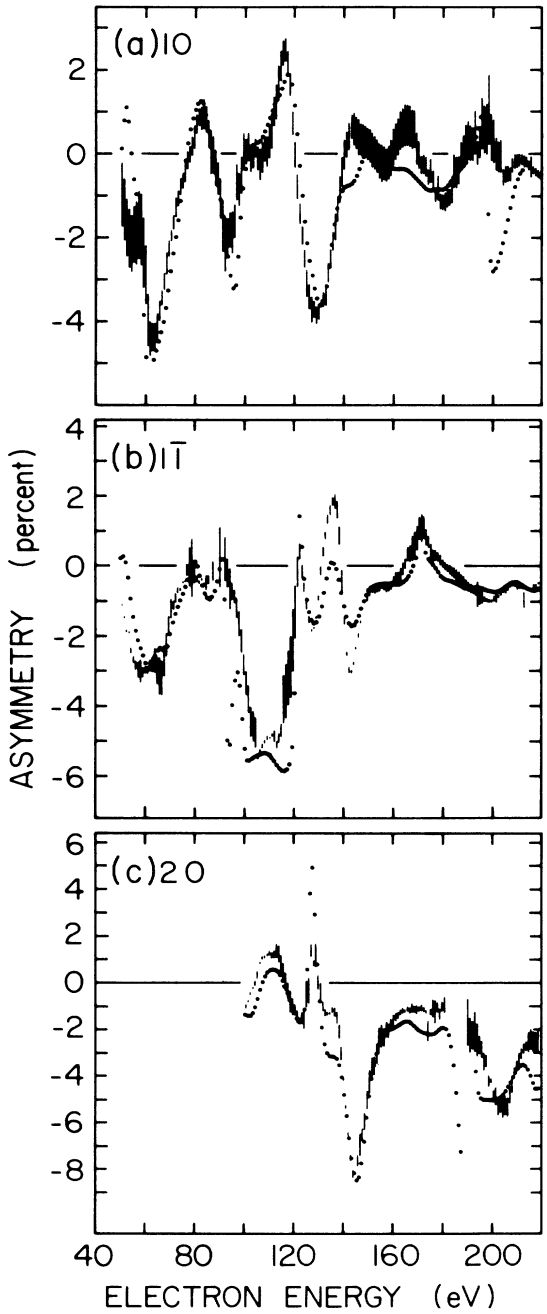

FIG. 3. *A-V* profiles for the 10, 20, and $1\bar{1}$ beams from Cu(100) at normal incidence. The 10 profile shown is the statistical average of the 10 and (inverted) $\bar{1}0$ data. The solid circles are the best theoretical fit to the data, which is obtained for $\Delta d_{12}=-1.2\%$, $\Delta d_{23}=+0.9\%$.

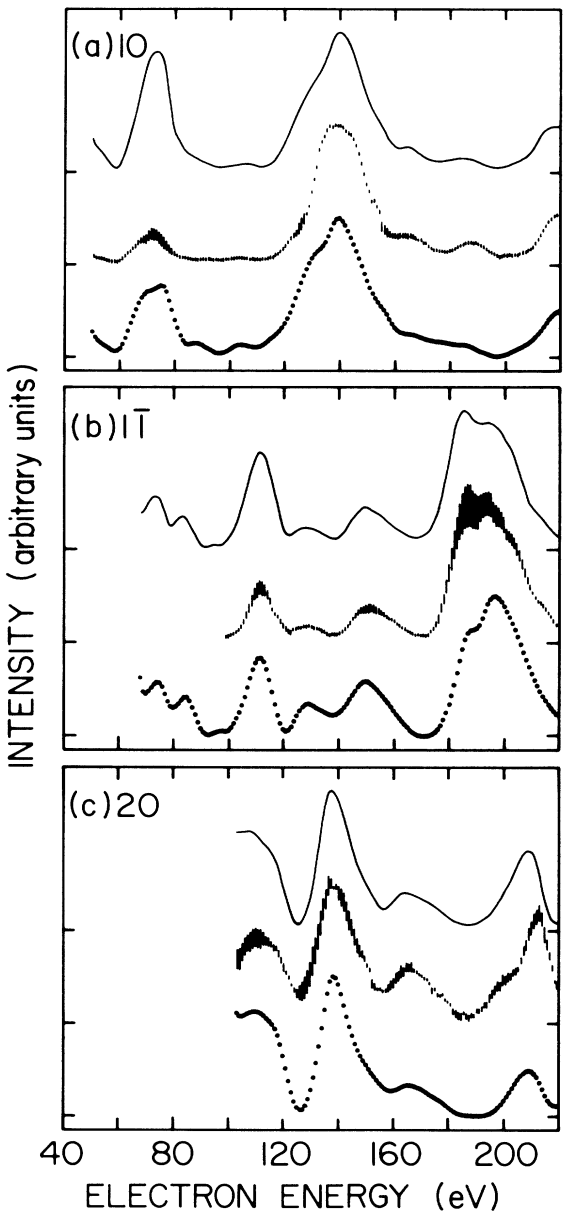

FIG. 4. *I-V* profiles for the 10, 20, and $1\bar{1}$ beams from Cu(100) at normal incidence. Vertical lines show present results; solid lines show measurements of Noonan and Davis (Refs. 4 and 5); dotted lines show profiles calculated for $\Delta d_{12}=-1.2\%$, $\Delta d_{23}=+0.9\%$.

sult because, in the present work, a small aperture was employed in the Faraday cup to minimize that part of the total Faraday cup current that resulted from diffuse scattering. In consequence, only a fraction of the total diffracted beam current is collected, and although this fraction is large it is somewhat energy dependent. As noted previously, however, such incomplete collection does not introduce systematic errors in the measurement of A-V profiles.

III. THEORY

To facilitate analysis of the experimental A-V profiles fully relativistic dynamical SPLEED calculations are undertaken. These calculations are based on the SPLEED theoretical formalism given by Feder,[7] although the present work differs in that multiple scattering between different atomic layers is treated using a newly developed spin-polarized extension[13] of the renormalized forward scattering (RFS) perturbation theory of Pendry.[14] An outline of the present theoretical approach is presented below. The notation used is the same as in an earlier review article by Feder,[7] to which the reader is referred for additional details.

As a starting point, the elastic scattering of electrons from a rigid "muffin-tin" sphere is considered. This is treated using a relativistic partial-wave analysis (see, for example, articles by Rose,[15] Kessler,[16] and Meister and Weiss[17]) that yields, for each orbital angular momentum quantum number $l>0$, two scattering phase shifts δ_l^+ and δ_l^- that relate to the total angular momentum quantum numbers $j=l+\frac{1}{2}$ and $j=l-\frac{1}{2}$, respectively. The influence of atomic vibrations on the scattering is approximated by use of effective phase shifts $\tilde{\delta}_l^{\pm}$ that are complex quantities obtained from $\delta_l^{\pm}$ by generalizing a spinless method proposed by Jepsen *et al.*[18] Values of $\tilde{\delta}_l^{\pm}$ may be derived using the expressions[7,19]

$$(l+1)\tilde{\varepsilon}_l^{+}+l\tilde{\varepsilon}_l^{-}=\sum_{l_1,l_2}B_{l_1l_2}[(l_1l_2l,000)]^2[(l_2+1)\varepsilon_{l_2}^{+}+l_2\varepsilon_{l_2}^{-}]\ , \tag{2a}$$

$$\tilde{\varepsilon}_l^{+}+\tilde{\varepsilon}_l^{-}=-\sum_{l_1,l_2}B_{l_1l_2}\left[\frac{(l_2+1)l_2}{(l+1)l}\right]^{1/2}(l_1l_2l,000)(l_1l_2l,0-11)(-\varepsilon_{l_2}^{+}+\varepsilon_{l_2}^{-})\ , \tag{2b}$$

where

$$\tilde{\varepsilon}_l^{\pm}=\tilde{\eta}_l^{\pm}-1=\exp(2i\tilde{\delta}_l^{\pm})-1\ , \tag{2c}$$

$$B_{l_1l_2}=(2l+1)(2l_1+1)i^{l_1}\times\exp(-2A_Tk^2)j_{l_1}(-2iA_Tk^2)\ , \tag{2d}$$

$$A_T=\frac{3\hbar^2}{2Mk_BT_D}\left[\frac{1}{4}+\left[\frac{T}{T_D}\right]^2\int_0^{T/T_D}\frac{x\,dx}{e^x-1}\right]\ . \tag{2e}$$

In these relations, the quantities (l_1l_2l,m_1m_2m) denote Wigner 3-j coefficients, $k=|\mathbf{k}|$, where $\mathbf{k}$ is the wave vector associated with the scattering electron, j_l is a spherical Bessel function, M is the mass of the atom corresponding to the muffin-tin potential, k_B is the Boltzmann constant, T is the surface temperature, and T_D the Debye temperature.

In the treatment of multiple scattering, as required in a dynamical theory, it is convenient to adopt a two-step approach in which the multiple scattering occurring within a particular atomic layer is first considered followed by consideration of multiple scattering between layers. The monochromatic wave field incident on a single layer centered at $z=0$ in the xy plane can be written in a plane-wave representation as

$$\sum_{\mathbf{g}}\sum_{s=\pm\frac{1}{2}}u_{\mathbf{g}s}^{\tau}\chi^s\exp(i\mathbf{k}_{\mathbf{g}}\cdot\mathbf{r})\ , \tag{3a}$$

where

$$\tau=\pm\ \text{ for } z\lesseqgtr 0\ , \tag{3b}$$

$$(\mathbf{k}_{\mathbf{g}}^{\tau})_x=(\mathbf{k}_0''+\mathbf{g})_x\ , \tag{3c}$$

$$(\mathbf{k}_{\mathbf{g}}^{\tau})_y=(\mathbf{k}_0''+\mathbf{g})_y\ , \tag{3d}$$

$$(\mathbf{k}_{\mathbf{g}}^{\tau})_z=\tau[2(E+V_0)-(\mathbf{k}_{\mathbf{g}}^{\tau})_x^2-(\mathbf{k}_{\mathbf{g}}^{\tau})_y^2]^{1/2}\ . \tag{3e}$$

In the above $\mathbf{g}$ denotes the reciprocal lattice vectors of the two-dimensional layer, χ^s are the Pauli basis spinors for spin up ($s=+\frac{1}{2}$) and spin down ($s=-\frac{1}{2}$), E is the energy (in vacuum) of the incident electron beam and $\mathbf{k}_0''$ its wave vector parallel to the surface, and V_0 is the complex inner potential. The incident wave field will scatter from the atomic layer resulting in a scattered wave field that can be expressed as

$$\sum_{\mathbf{g}}\sum_{s=\pm\frac{1}{2}}v_{\mathbf{g}s}^{\tau}\chi^s\exp(i\mathbf{k}_{\mathbf{g}}^{\tau}\cdot\mathbf{r})\ , \tag{4a}$$

with

$$\tau=\mp\ \text{ for } z\lesseqgtr 0\ . \tag{4b}$$

The expansion coefficients in Eq. (4a) are related to those in Eq. (3a) by

$$v_{\mathbf{g}s}^{\tau}=\sum_{\tau'=\pm}\sum_{\mathbf{g}'}\sum_{s'=\pm\frac{1}{2}}M_{\mathbf{g}\mathbf{g}'ss'}^{\tau\tau'}u_{\mathbf{g}'s'}^{\tau'}\ , \tag{5}$$

where the scattering matrix elements are given by

$$M_{\mathbf{g}\mathbf{g}'ss'}^{\tau\tau'}=\delta_{\mathbf{g}\mathbf{g}'ss'}^{\tau\tau'}+\frac{4\pi^2}{kA(k_{\mathbf{g}}^{+})_z}\sum_{\kappa,\mu}\tilde{\varepsilon}_l^{\kappa}\sum_{\kappa',\mu'}i^{l'}C(l'\tfrac{1}{2}j';\mu'-s,s)(-1)^{\mu'-s}\times Y_{l'}^{-\mu'+s}(\hat{\mathbf{k}}_{\mathbf{g}}^{\tau})(1-X)_{\kappa'\mu'\kappa\mu}^{-1}C(l\tfrac{1}{2}j;\mu-s',s')i^{-l}Y_l^{\mu-s'}(\hat{\mathbf{k}}_{\mathbf{g}}^{\tau})\ , \tag{6}$$

which is similar to Eq. (33) of Feder,[7,19] use having been made of the relation

$$[Y_l^m(\theta,\phi)]^* = (-1)^m Y_l^{-m}(\theta,\phi) \ . \tag{7}$$

The matrix X is defined by Eq. (30) of Feder,[7] in which, however, $C(l'\frac{1}{2}j';\mu-s,s)$ must be replaced by $C(l'\frac{1}{2}j';\mu'-s,s)$. The index κ is related to the total quantum number j by

$$\kappa=-(l+1) \quad \text{for } j=l+\tfrac{1}{2}$$

and

$$\kappa=l \quad \text{for } j=l-\tfrac{1}{2} \ , \tag{8}$$

and μ can take the values $-j, -j+1, \ldots, j$. The definition of $\tilde{\varepsilon}_l^\kappa$ follows from Eqs. (2), the C's are Clebsch-Gordan coefficients, A is the area of the layer unit cell, $\hat{\mathbf{k}}_{\mathbf{g}}^{\tau}$ is a unit vector in the direction of $\mathbf{k}_{\mathbf{g}}^{\tau}$ [a vector with complex components defined by Eqs. (3) which thus requires use of Eq. (7)] and $\delta_{\mathbf{g}\mathbf{g}'ss'}^{\tau\tau'}$ is a Kronecker-type symbol equal to unity if $\tau=\tau'$, $g=g'$, and $s=s'$ and zero otherwise.

The results describing scattering by individual atomic layers are used in obtaining the elements of the (2×2) scattering matrices $S_{\mathbf{g}}$ that relate scattering, by the whole surface, of an incident beam into the diffracted beam $\mathbf{g}$ via expressions of the form

$$v_{\mathbf{g}}=S_{\mathbf{g}}u_0 \ , \tag{9a}$$

$$\begin{bmatrix} v_1 \\ v_2 \end{bmatrix} = \begin{bmatrix} S_{11} & S_{12} \\ S_{21} & S_{22} \end{bmatrix} \begin{bmatrix} u_1 \\ u_2 \end{bmatrix} \ , \tag{9b}$$

where u_0 is a Pauli spinor representation of the incident wave field and $v_{\mathbf{g}}$ is a spinor representation of that part of the total reflected wave field that is elastically diffracted into the beam $\mathbf{g}$. In calculating the matrix elements of $S_{\mathbf{g}}$ multiple scattering between different layers is treated using a spin-polarized generalization[13] of the RFS perturbation theory of Pendry.[14] That is, an assumed incident wave field is propagated from the vacuum to the first atomic layer, and then between deeper layers, either inwardly or outwardly, by use of propagation matrices $P^{\pm}$ of the type defined by Eqs. (5.26) in the book of Pendry.[20] The scattering of a wave field incident upon a particular atomic layer, either inwardly on its top or outwardly on its bottom, is calculated by use of Eq. (5). These procedures are performed, in a perturbative sequence, order-by-order in the coefficients of the wave field, until adequate convergence of the calculated wave field that propagates outwardly from the surface atomic layer is achieved. Although this spin-polarized application of RFS is reasonably straightforward, detailed tests were undertaken to evaluate its convergence properties and, hence, accuracy. These tests will be described in detail elsewhere.[13] SPLEED calculations, however, require two separate applications of RFS at each electron energy; one to determine the elements S_{11} and S_{21} of Eq. (9b), the other S_{12} and S_{22}. The final, rather lengthy computer codes were checked for correctness by using them to calculate A-V profiles for W(001)-(1×1) and visually comparing the results with corresponding calculated profiles available in the literature.[21–23] Tests were also conducted to ensure that numerical convergence was achieved with the number of beams, the number of phase shifts, the depth of electron beam penetrates the crystal, and the number of passes of RFS. At the highest energies ($\sim$220 eV) considered in the present calculations 49 beams (i.e., the number of $\mathbf{g}$'s used in RFS) and 10 nonrelativistic (or 19 relativistic) phase shifts were employed. The incident electron beam was allowed to penetrate into the crystal to a depth such that backscattering from the 14th atomic layer was included in the RFS calculations, and five to seven passes (or perturbation orders) of RFS theory were typically performed.

IV. DISCUSSION

To calculate A-V profile both structural and nonstructural parameters must be specified. Earlier LEED intensity analysis of Cu(100) suggested that the following nonstructural parameters are appropriate, namely a surface region Debye temperature of 330 K, a truncated free atom potential with full Slater exchange, an imaginary component of the optical potential equal to $0.85E^{1/3}$ eV (with E in eV) and a nonreflecting surface barrier (see, for example, Jepsen *et al.*[18] and Feder and Kirschner[23]). To test the sensitivity of calculated A-V profiles to the exact choice of nonstructural parameters, A-V profiles were calculated as the imaginary component of the optical potential and the Debye temperature were varied about the values quoted above. Calculations were also performed using the Cu band-structural potential of Moruzzi *et al.*[24] These calculations, although not totally exhaustive, indicated that the calculated A-V profiles are rather insensitive to the choice of nonstructural parameters, and the parameters derived from the earlier LEED intensity analyses were deemed adequate for the purposes of the present study.

The sensitivity of calculated A-V profiles to the choice of structural parameters is illustrated in Figs. 5 and 6. Since earlier LEED intensity analyses suggest that Cu(100) undergoes multilayer relaxation but not reconstruction, the structural parameters varied in generating these figures are the spacing d_{12} between the first and second atomic layers and the spacing d_{23} between the second and third layers. Figure 5 shows the changes in the computed 10 beam A-V profiles that result as d_{12} as varied relative to the bulk interlayer spacing (1.808 Å) by amounts Δd_{12} ranging from $+4\%$ to -6%, keeping d_{23} equal to the bulk spacing. The influence of changes in d_{23} on the calculated A-V profiles is illustrated in Fig. 6 for a comparable range of variations, Δd_{23}, in the second interlayer spacing. In these calculations the top interlayer spacing d_{12} is taken to be contracted by 1% relative to the bulk spacing. It is apparent from Figs. 5 and 6 that calculated A-V profiles are quite sensitive to the choice of structural parameters, demonstrating the utility of SPLEED measurements in structure determinations.

In order to optimize the choice of surface structural parameters it is necessary to optimize the fit of the calculated A-V profiles to the experimental data. To accomplish this an R-factor analysis similar to those employed in the interpretation of LEED I-V data was undertaken.[1–5] R factors based on several different criteria have been defined for use in LEED studies.[1–5] In the present work a

simple, single-beam R factor R_i defined by

$$R_i = \frac{\sum_{n=1}^{N_i} (A_n^{\text{calc}} - A_n^{\text{expt}})^2}{\sum_{n=1}^{N_i} (A_n^{\text{expt}})^2} \tag{10}$$

is employed where A_n^{calc} and A_n^{expt} are the calculated and experimental spin-asymmetry parameters, respectively, at each of the N_i energies n included in the experiment and theory comparison. This R factor is analogous to the $R2$ R factor defined by Van Hove *et al.*[2] for use in LEED intensity analyses, except that *no constant is included to scale the calculated and experimental profiles.* Although

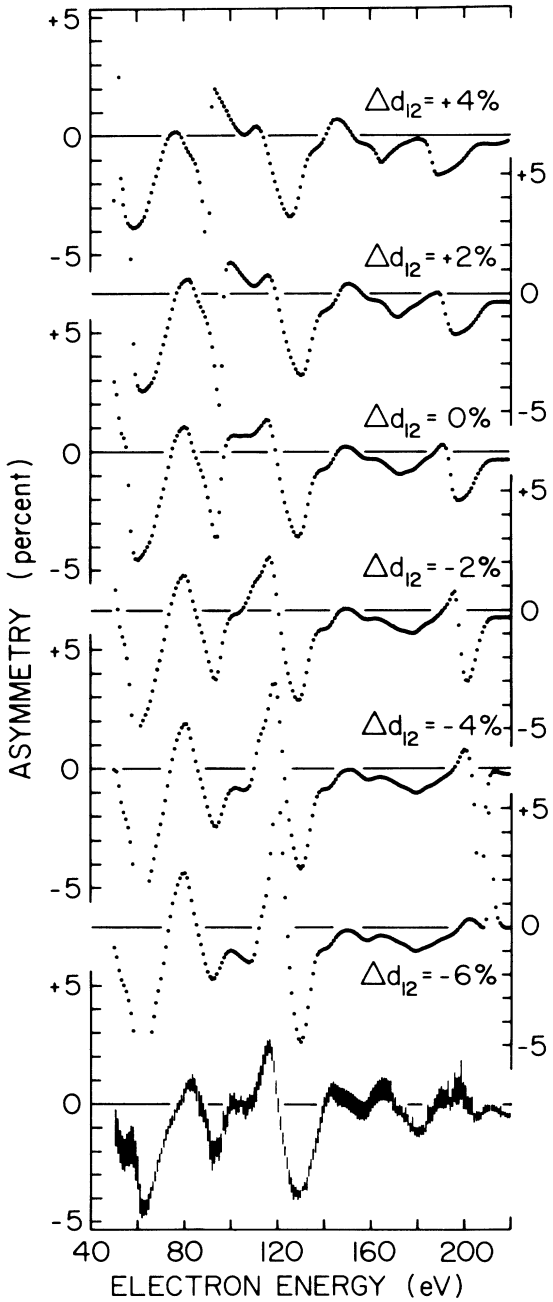

FIG. 5. Sensitivity of the calculated 10 beam A-V profiles to changes Δd_{12} in the spacing d_{12} between the first and second layers relative to the bulk interlayer spacing. These calculations assume a second interlayer spacing d_{23} equal to that in the bulk. For comparison purposes the measured A-V profile is also included.

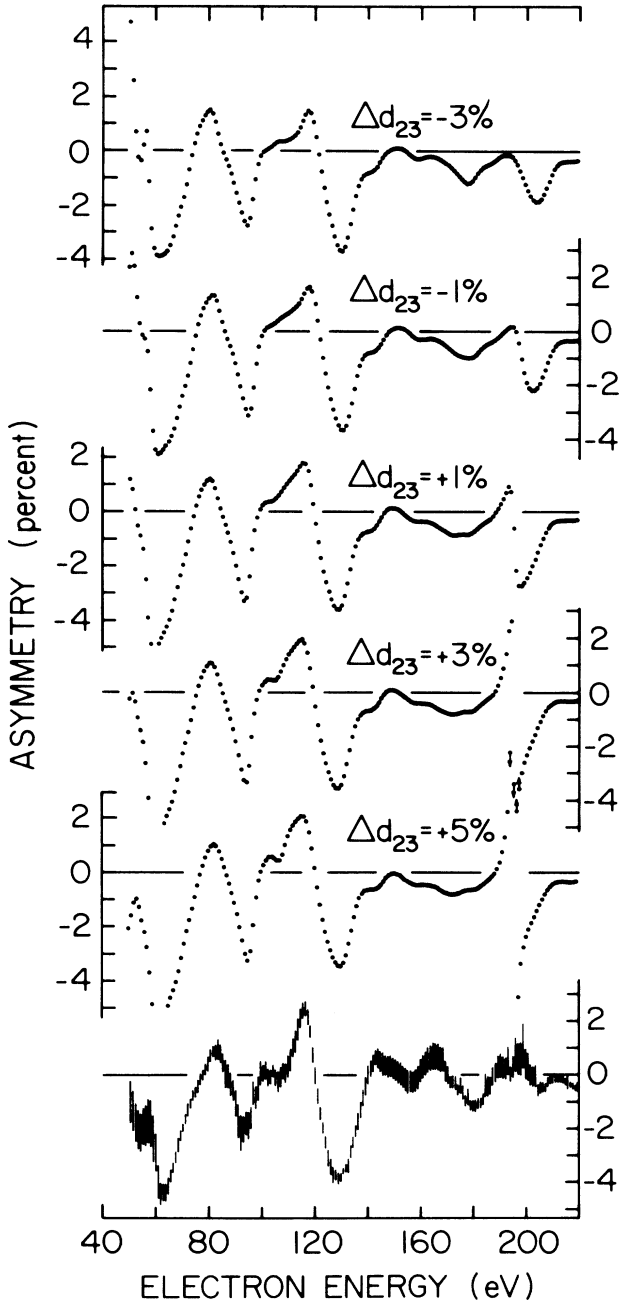

FIG. 6. Sensitivity of the calculated 10 beam A-V profiles to changes Δd_{23} in the spacing d_{23} between the second and third atomic layers relative to the bulk interlayer spacing. These calculations assume a top interlayer spacing d_{12} contracted by $\Delta d_{12} = -1\%$ relative to the bulk. For comparison purposes the measured A-V profile is also included.

TABLE I. The sensitivity of the total and single-beam R factors to variations in structural parameters.

Structural parameters		Single beam R-Factors			
Δd_{12}	Δd_{23}	10 beam	$1\bar{1}$ beam	20 beam	Total R factor
+4%	0%	0.249	0.113	0.295	0.215
+2%	0%	0.182	0.076	0.231	0.159
0%	0%	0.120	0.076	0.199	0.126
−2%	0%	0.077	0.101	0.192	0.116
−4%	0%	0.065	0.143	0.221	0.133
−6%	0%	0.103	0.214	0.291	0.190
−1%	−3%	0.096	0.118	0.270	0.150
−1%	−1%	0.094	0.089	0.212	0.123
−1%	+1%	0.099	0.090	0.179	0.117
−1%	+3%	0.116	0.124	0.175	0.134
−1%	+5%	0.139	0.198	0.199	0.175

selection of the present R factor is somewhat arbitrary, use of a systematic R factor analysis represents a major advance in the use of SPLEED data for surface structure determinations. In determining R_i the summation over energy was restricted to regions where the calculated intensity of the diffracted beam is $\geq 0.001\%$ of the incident beam intensity and where the standard deviation about the mean of the measured asymmetries is $\leq \pm 0.02$. The first condition removes from consideration regions in which numerical convergence of the calculated values is difficult to achieve, the second excludes data points for which the experimental uncertainties are large. Although these selection criteria are rather arbitrary, tests showed that the present structural conclusions were not significantly altered by the use of any other reasonable selection criteria.

As demonstrated in Table I, the single-beam R factors are quite sensitive to changes in the structural parameters d_{12} and d_{23}. This sensitivity is greater than that noted in earlier R-factor analyses of LEED I-V profiles for Cu(100). (The R factors in Table I pertain to the same structural parameters as used when deriving the A-V profiles shown in Figs. 5 and 6.) As apparent from Table I, optimum fits to the data for each beam studied are obtained with somewhat different assumed surface structures. These differences are similar in magnitude to those noted when analyzing different LEED I-V profiles.[4] In an attempt to optimize the choice of structural parameters, the *overall* fit between the calculated and experimental A-V profiles was evaluated by use of a multibeam R-factor R, defined as

$$R = \sum_i N_i R_i / \sum_i N_i \tag{11}$$

where the summation ranges over the i different beams for which data are available, i.e., the 10, 20, and $1\bar{1}$ beams. This total R factor weights the contributions from each of the beams according to the number of energies in each at which comparisons are made. Total three-beam R factors are included in Table I and this parameter is minimized with choice of a top interlayer spacing d_{12} contracted relative to the bulk by an amount $\Delta d_{12} = -1.2\%$ and a second interlayer spacing d_{23} that is expanded relative to the bulk by $\Delta d_{23} = +0.9\%$. A-V (and I-V) profiles computed using these parameters are included in Figs. 3 and 4 and provide a good fit to the experimental data. That a fit of this quantity is achieved in the A-V profiles demonstrates that the SPLEED theory employed embodies all the pertinent physics. The present fit is also obtained without the use of any scaling factors such as applied in the case of LEED I-V analyses, where the experimentally determined intensities are typically well below those expected theoretically. This discrepancy is thought to result from incoherent scattering by surface defects, such as steps, which enhances the diffuse background at the expense of the diffracted beam intensities. This study shows that A-V profiles, on the other hand, are insensitive to the presence of such effects.

The surface structure derived from analysis of the SPLEED measurements ($\Delta d_{12} = -1.2\%$, $\Delta d_{23} = +0.9\%$) is in accord with that determined from earlier LEED intensity analysis ($\Delta d_{12} = -1.1\%$, $\Delta d_{23} = +1.7\%$).[4] Since calculated A-V and I-V profiles depend differently on the assumed structural and nonstructural parameters, this agreement reinforces the earlier conclusion that multilayer relaxation, but not reconstruction, is present at the Cu(100) surface, and that such relaxations are small. The present work clearly demonstrates that combined measurements of spin-asymmetry and intensity profiles using SPLEED should provide an improved basis for surface structure determinations on surfaces of greater complexity, such as reconstructed surfaces.

ACKNOWLEDGMENTS

The research of D.M.L., F.B.D., and G.K.W. is supported by the Division of Materials Sciences, U.S. Department of Energy and the Robert A. Welch Foundation. That of H.L.D. is partially sponsored by the Division of Materials Sciences, U.S. Department of Energy under Contract No. DE-AC05-84OR21400 with Martin Marietta Energy System, Inc.

*Present address: Metal Physics Branch, Naval Research Laboratory, Washington, D.C. 20375.
[1]F. Zanazzi and F. Jona, Surf. Sci. **62**, 61 (1977).
[2]M. A. Van Hove, S. Y. Tong, and M. H. Econin, Surf. Sci. **64**, 85 (1977).
[3]E. Zanazzi, U. Bardi, and M. Maglietta, J. Phys. C **13**, 4001 (1980).
[4]H. L. Davis and J. R. Noonan, J. Vac. Sci. Technol. **20**, 842 (1982).
[5]J. R. Noonan and H. L. Davis, J. Vac. Sci. Technol. **17**, 194 (1980).
[6]D. T. Pierce, R. J. Celotta, G. C. Wang, W. N. Unertl, A. Galejs, C. E. Kuyatt, and S. R. Mielczarek, Rev. Sci. Instrum. **51**, 478 (1980).
[7]R. Feder, J. Phys. C **14**, 2049 (1981), and references therein.
[8]A preliminary report on this work is contained in D. M. Lind, K. D. Jamison, F. B. Dunning, G. K. Walters, and H. L. Davis, J. Vac. Sci. Technol. A **4**, 1271 (1986).
[9]Data for the specular beam is also available: D. M. Lind, Ph.D. thesis, Rice University, 1986.
[10]K. D. Jamison, D. M. Lind, F. B. Dunning, and G. K. Walters, Surf. Sci. **159**, L451 (1985).
[11]M. Kalisvaart, M. R. O'Neill, T. W. Riddle, F. B. Dunning, and G. K. Walters, Phys. Rev. B **17**, 1570 (1978).
[12]R. Feder, Phys. Lett. **78A**, 103 (1980).
[13]H. L. Davis (unpublished).
[14]J. B. Pendry, J. Phys. C **4**, 3095 (1971).
[15]M. E. Rose, *Relativistic Electron Theory* (Wiley, New York, 1961).
[16]J. Kessler, *Polarized Electrons* (Springer-Verlag, Berlin, 1976).
[17]H. J. Meister and H. F. Weiss, Z. Phys. **216**, 165 (1968).
[18]D. W. Jepsen, P. M. Marcus, and F. Jona, Phys. Rev. B **5**, 3933 (1972).
[19]Minor typographical errors present in Ref. 7 have been corrected—see footnotes in E. Tamura, B. Ackermann, and R. Feder, J. Phys. C **17**, 5455 (1984).
[20]J. B. Pendry, *Low Energy Electron Diffraction* (Academic, New York, 1974).
[21]R. Feder, P. J. Jennings, and R. O. Jones, Surf. Sci. **61**, 307 (1976).
[22]R. Feder, Surf. Sci. **63**, 283 (1977).
[23]R. Feder and J. Kirschner, Surf. Sci. **103**, 75 (1981).
[24]V. L. Moruzzi, J. F. Janak, and A. R. Williams, *Calculated Electronic Properties of Metals* (Pergamon, New York, 1978).